NANO LETTERS

Letter

pubs.acs.org/NanoLett

Snapshots of Dirac Fermions near the Dirac Point in Topological Insulators

C. W. Luo,*[,†] H. J. Wang,[†] S. A. Ku,[†] H.-J. Chen,[†] T. T. Yeh,[†] J.-Y. Lin,*[,‡] K. H. Wu,[†] J. Y. Juang,[†] B. L. Young,[†] T. Kobayashi,[†,§] C.-M. Cheng,[∥] C.-H. Chen,[∥] K.-D. Tsuei,[∥] R. Sankar,[⊥] F. C. Chou,[⊥] K. A. Kokh,[¶,#] O. E. Tereshchenko,[#,○] E. V. Chulkov,[●,♦] Yu. M. Andreev,[□,■] and G. D. Gu[△]

[†]Department of Electrophysics and [‡]Institute of Physics, National Chiao Tung University, Hsinchu, Taiwan

[§]Advanced Ultrafast Laser Research Center, and Department of Engineering Science, Faculty of Informatics and Engineering, University of Electro-Communications, 1-5 1 Chofugaoka, Chofu, Tokyo 182-8585, Japan

[∥]National Synchrotron Radiation Research Center, Hsinchu, Taiwan

[⊥]Center for Condensed Matter Sciences, National Taiwan University, Taipei 106 Taiwan

[¶]Institute of Geology and Mineralogy, SB RAS, Novosibirsk, Russia

[#]Novosibirsk State University, 2, Pirogov str. Novosibirsk 630090, Russia

[○]Institute of Semiconductor Physics, Novosibirsk, Russia

[●]Donostia International Physics Center, Departamento de Fisíca. de Materiales UPV/EHU, Centro de Fisíca. de Materiales CFM-MPC and Centro Mixto CSIC-UPV/EHU, Donostia-San Sebastián, Basque Country, Spain

[□]Institute of Monitoring of Climatic and Ecological Systems of Siberian Branch of Russian Academy of Sciences, Tomsk, Russia

[■]Siberian Physical-Technical Institute of Tomsk State University, 634050, Tomsk, Russia

[△]Condensed Matter Physics and Materials Science Department, Brookhaven National Laboratory, Upton, New York 11973, United States

[♦]Tomsk State University, 634050, Tomsk, Russia

S *Supporting Information*

ABSTRACT: The recent focus on topological insulators is due to the scientific interest in the new state of quantum matter as well as the technology potential for a new generation of THz optoelectronics, spintronics and quantum computations. It is important to elucidate the dynamics of the Dirac fermions in the topologically protected surface state. Hence we utilized a novel ultrafast optical pump mid-infrared probe to explore the dynamics of Dirac fermions near the Dirac point. The femtosecond snapshots of the relaxation process were revealed by the ultrafast optics. Specifically, the Dirac fermion-phonon coupling strength in the Dirac cone was found to increase from 0.08 to 0.19 while Dirac fermions were away from the Dirac point into higher energy states. Further, the energy-resolved transient reflectivity spectra disclosed the energy loss rate of Dirac fermions at room temperature was about 1 meV/ps. These results are crucial to the design of Dirac fermion devices.

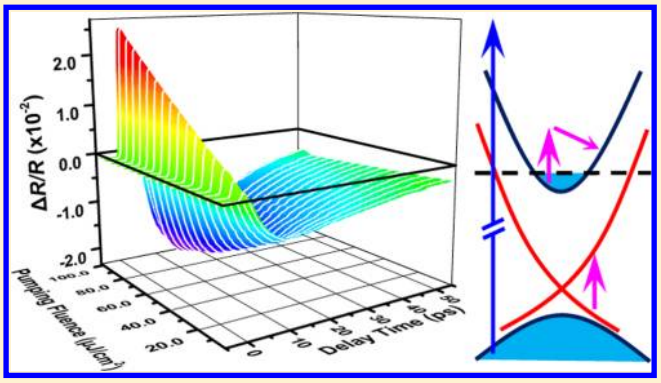

KEYWORDS: *Topological insulator, ultrafast optical pump mid-infrared probe spectroscopy, Dirac fermion dynamics, Dirac fermion-phonon coupling*

The discovery of 3D topological insulators (TIs)[1] initiated a new era of condensed matter physics.[2,3] As Dirac fermions plays a crucial role in determining the performances of any real TI devices, a better understanding of the bulk state and the surface state,[4−14] and the coupling mechanisms between them, is imperative. From a practical point of view, contact-free optical techniques, such as second harmonic generation,[11] terahertz time-domain spectroscopy,[15] UV−visible−IR reflectance and transmission spectroscopy,[16] and optical pump−probe spectroscopy,[17−21] would be the most feasible schemes to investigate the characteristics of TIs. However, the surface signatures are easily overwhelmed by the bulk contributions. Recent TrARPES studies have shown the surface carrier

Received: June 16, 2013
Revised: October 21, 2013
Published: November 14, 2013

ACS Publications © 2013 American Chemical Society

population in TIs can be induced by photoexcitation[12,13] and can separately obtain the temperature and chemical potential relaxation of both the surface and the bulk.[14] Nevertheless, the ultrafast behavior of Dirac fermions near the Dirac point and their detailed energy-dependent coupling with phonons remain elusive for lack of probes with the appropriate energy range (~100 meV) specific to the Dirac cone. We further take the advantage of the appropriate probe photon energies in the optical pump mid-infrared probe (OPMP) spectroscopy to explore the nonequilibrium dynamics of TIs. The mid-infrared photon energy range (87−153 meV < bandgap energy of 300 meV in Bi_2Se_3) naturally selects the transitions limited within the Dirac cone, and the femtosecond-time and millielectron-volt-energy resolution allows us to distinguish the individual dynamics of both the surface and the bulk. Such ultrafast mid-infrared approach has potentially provided significant insights to other correlation physics in strongly correlated materials, for example, electronic phase transition in $BaFe_2As_2$ superconductors[22] and phonon resonances in optimally doped $YBa_2Cu_3O_{7-\delta}$.[23]

Figure 1 provides a synopsis of the OPMP spectra for all samples investigated. The doping levels of samples span a wide

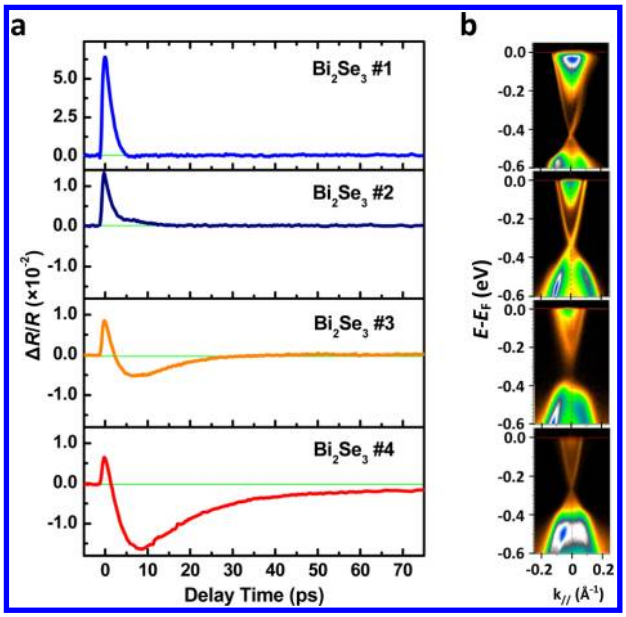

Figure 1. Carrier concentration (n) dependence of the transient change in reflectivity $\Delta R/R$ in Bi_2Se_3 single crystals. (a) $\Delta R/R$ of samples #1 ($n = 51.5 \times 10^{18}$ cm^{-3}), #2 ($n = 13.9 \times 10^{18}$ cm^{-3}), #3 ($n = 5.58 \times 10^{18}$ cm^{-3}), and #4 ($n = 0.25 \times 10^{18}$ cm^{-3}) with a pumping fluence of 34 μJ/cm^2 and probing photon energy of 141 meV. (b) ARPES band dispersion images on samples of (a).[24]

range, as listed in Table 1, (#1: $n = 51.5 \times 10^{18}$ cm^{-3}, #2: $n = 13.9 \times 10^{18}$ cm^{-3}, #3: $n = 5.58 \times 10^{18}$ cm^{-3}, #4: $n = 0.25 \times 10^{18}$ cm^{-3}) and show corresponding ARPES images.[24] Details of Bi_2Se_3 single crystal preparation and the OPMP spectroscopy can be found in the Supporting Information. For the case of Bi_2Se_3 #1 with a high carrier concentration ($n = 51.5 \times 10^{18}$ cm^{-3}), a positive peak is clearly observed in $\Delta R/R$. This positive peak gradually diminishes as n decreases (#1→#4 in Figure 1a). Noticeably, an additional negative peak appears for the cases of $n = 5.58 \times 10^{18}$ cm^{-3} and $n = 0.25 \times 10^{18}$ cm^{-3}, and its amplitude is inversely proportional to n.

Table 1. Fermi Energy and Carrier Concentration of Bulk and Surface States for Various Samples Grown by Different Methods ([a]Vertical Bridgman, [b] Modified Floating Zone)[a]

		carrier concentration		
code	$E_F - E_{Dirac\ point}$ (meV)	n_{bulk} (10^{18} cm^{-3})	$n_{surface}$ (10^{13} cm^{-2})	$n_{surface}/(n_{surface}+n_{bulk}d)$
#1 [a]	422	−51.5 ± 0.84	−1.45	0.11
#2 [b]	325	−13.9 ± 0.26	−0.83	0.20
#3 [a]	284	−5.58 ± 0.25	−0.72	0.35
#4 [b]	260	−0.25 ± 0.01	−0.47	0.89

[a]All samples are n-type. "d = 23.5 nm" is the penetration depth of 800-nm pumping light (see Supporting Information).

To elucidate the origins of both the positive and negative signals, a model is shown in Figure 2a for the optical pumping (1.55 eV) and mid-infrared probing processes in the schematic energy band structure of the TIs based on the ARPES image in Figure 1b. Because the used probe photon energy (87−153 meV) of the mid-infrared (mid-IR) is much smaller than the band gap of ~300 meV in Bi_2Se_3 (as shown in the ARPES images of Figure 1b), the interband transitions between the valence band (VB) and the conduction band (CB) of the bulk are not allowed to occur. Thus, the free carrier absorption in the CB (mid-IR probe (1) in Figure 2a) and Dirac cone surface state (mid-IR probe (2) in Figure 2a) will dominate the probe processes, which are responsible for the positive and negative peaks in $\Delta R/R$, respectively. To confirm this assignment and reveal the physical meanings of the positive peak in $\Delta R/R$, the photon energy dependence of $\Delta R/R$ for #1 sample is shown in Figure 2b. By decreasing the photon energy, $\Delta R/R$ gradually changes from positive to negative. Around 136 meV (1100 cm^{-1}), there are some intermediate signals mixed with both positive and negative peaks, corresponding to deep in the Fourier transform infrared (FTIR) reflectance spectrum (the inset of Figure 2b). After pumping, the excited carriers suffer the so-called intervalley scattering (see Supporting Information), leading to the redshift of the reflectance spectra. Therefore, the reflectivity increases as a function of time with a large probing photon energy, which is higher than the position of 136 meV deep in the reflectance spectra due to plasma edge. On the contrary, the reflectivity decreases as a function of time with a small probing photon energy, which is lower than the position of 136 meV deep in the reflectance spectra. Similar results were also observed in a typical semiconductor n-type GaAs.[25]

Comparing the $\Delta R/R$ curves and ARPES images in Figure 1, the amplitude of the positive peak in $\Delta R/R$ gradually shrinks as the bulk carrier concentration decreases (see Table 1). On the other hand, the negative peak in $\Delta R/R$ increases as the bulk and surface carrier concentrations decrease. However, the negative peak of $\Delta R/R$ increases dramatically with an increasing ratio of the surface carrier concentration to the total carrier concentration [$n_{surface}/(n_{surface}+ n_{bulk}d)$ in Table 1], implying an intimate relation between the negative peak of $\Delta R/R$ and Dirac fermions. Besides, the $\Delta R/R$ signal significantly depends on the pumping fluences shown in Figure 3a. Interestingly, the positive peak of $\Delta R/R$ has a stronger dependence on the pumping fluences than the negative peak does. Therefore, the negative peak still subsists at the low pumping fluence of 3.3 μJ/cm^2,[26] while the positive peak almost vanishes. This means the mid-IR probe process (1) in the bulk state (see Figure 2a) can be suppressed by reducing

dx.doi.org/10.1021/nl4021842 | Nano Lett. 2013, 13, 5797−5802

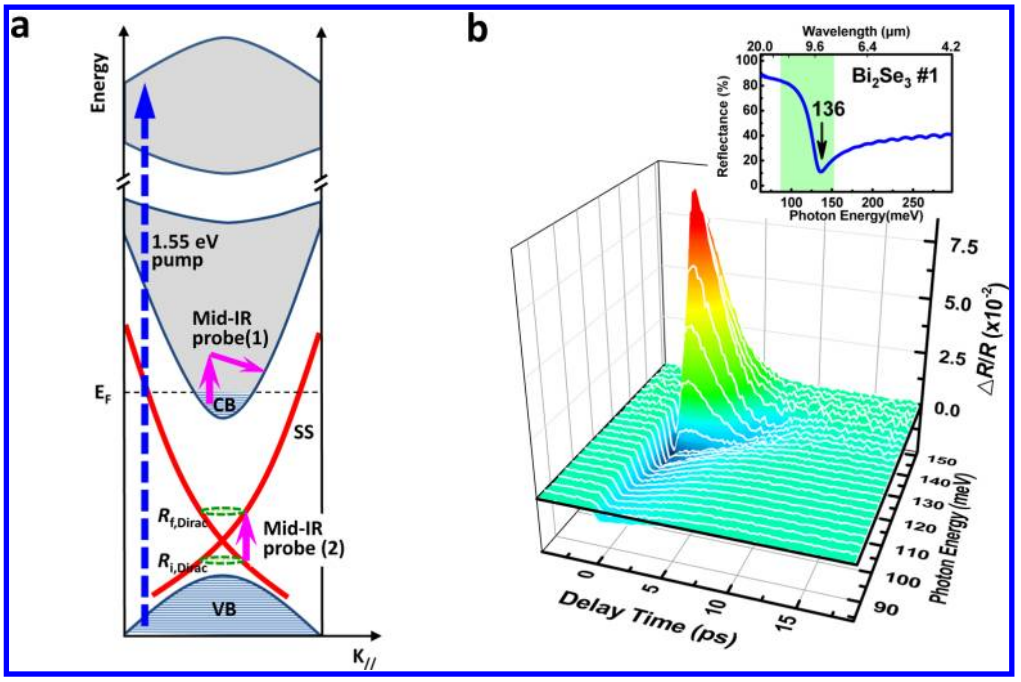

Figure 2. Schematic energy band structure and photon energy dependence of $\Delta R/R$ in a bulk state. (a) Schematic energy band structure of TIs according to the ARPES images in Figure 1b and the optical pump mid-IR probe processes. CB: conduction band. VB: valence band. SS: surface state. $R_{i,Dirac}$ and $R_{f,Dirac}$: the circumferences of initial and final states in Dirac cone for mid-IR probing. (b) With a pumping fluence of 38 μJ/cm^2, the $\Delta R/R$ of Bi_2Se_3 #1 at various photon energies (wavenumber) from 87−153 meV (700−1234 cm^{-1}). Inset: the Fourier transform infrared (FTIR) reflectance spectrum of Bi_2Se_3 #1. The gray area indicates the range of the mid-IR photon energy used in this study.

the pumping fluences; meanwhile, the mid-IR probe process (2) (see Figure 2a) associated with the negative peak can be preserved at the low pumping fluence (see Supporting Information). Here, we can conclude that the positive (or negative) signal within a several picoseconds time scale in $\Delta R/R$ is due to the process (1) of the mid-IR probe in the bulk state of Bi_2Se_3.

The relation between the negative peak and Dirac fermions can be certified in a quantitative way. According to the Fermi Golden rule, the amplitude of the negative peak should be proportional to the transition probability ($T_{i\rightarrow f}$) between the initial and final density of states in the Dirac cone. With an increase in the probing photon energy, the amplitude of the negative peak increases. Owing to the large positive signal before 5 ps in samples #1 and #2, this probing photon energy dependence of the negative peak amplitude cannot be easily disclosed. However, this dependence was clearly observed in both samples #3 and #4. The experimental data are fitted well by the $R_{i,Dirac} \times R_{f,Dirac}$ (dashed line in Figure 3c, $R_{i,Dirac}$ and $R_{f,Dirac}$ are the circumferences of rings in Figure 2a), which is proportional to the transition rate between the initial and final density of states for the mid-IR probe process (2) in the Dirac cone (see Supporting Information). This strongly indicates the negative peak of $\Delta R/R$ is dominated by the mid-IR probe process (2) in the Dirac cone (see Figure 2a). Consequently, the ultrafast dynamics of the Dirac fermions can be clearly disclosed by the negative peak of $\Delta R/R$. The above experiments were carried out at the low pumping fluence of 3.3 μJ/cm^2 to avoid disturbance of the positive peak from the bulk state, as shown in Figure 3b.

The rising time (τ_r) and decay time (τ_d) of the negative peak of $\Delta R/R$ significantly depends on the probing photon energy, as in Figure 3d. The rising time of the negative peak of $\Delta R/R$ also becomes longer when the probed regime is closer to the Dirac point. On the basis of the above observations, we can further establish the ultrafast relaxation picture for Dirac fermions in TIs. Immediately following the 1.55 eV pumping, the major process is the carriers in the bulk valence band (BVB) are excited to the bulk conduction band (BCB). The carrier recombination between the BCB and BVB can be ignored in this study due to the time scale for such a process is typically ≫1 ns.[27] Consequently, the unoccupied states in BVB caused by pumping would mainly be refilled through the bottom part of the upper Dirac cone that almost overlaps with the top of BVB at the same momentum space, as shown in the ARPES images of Figure 1b. This implies the carriers in this part of the Dirac cone can be easily transferred into the unoccupied states in BVB and increasing the number of the unoccupied states near the Dirac point enhances the absorption channel for the mid-IR process (2) in the Dirac cone (Figure 2a). Therefore, the reflectivity of the mid-IR probing light decreases within 1.47−3.60 ps, that is, the rising time of the negative peak in Figure 3b,d. Once the carriers in the Dirac cone relax into BVB, the BCB (like a carrier reservoir) subsequently injects the excited carriers into the unoccupied states in the Dirac cone to diminish the absorption channel for the mid-IR process (2) (Figure 2a). This leads to the increased mid-IR reflectivity within 14.8−87.2 ps, consistent with the ARPES results[12,13] of a nonequilibrium population of the surface state persisting for >10 ps. The several tens of picoseconds in decay time, which is much longer than the rising time of several picoseconds, is because the carriers in BCB cannot directly transfer into the top of the Dirac cone without overlaps occurring between them and other auxiliaries, for example, phonons. A movie showing the relaxation processes of Dirac fermions in the Dirac cone after pumping is included in the Supporting Information.

dx.doi.org/10.1021/nl4021842 | Nano Lett. 2013, 13, 5797−5802

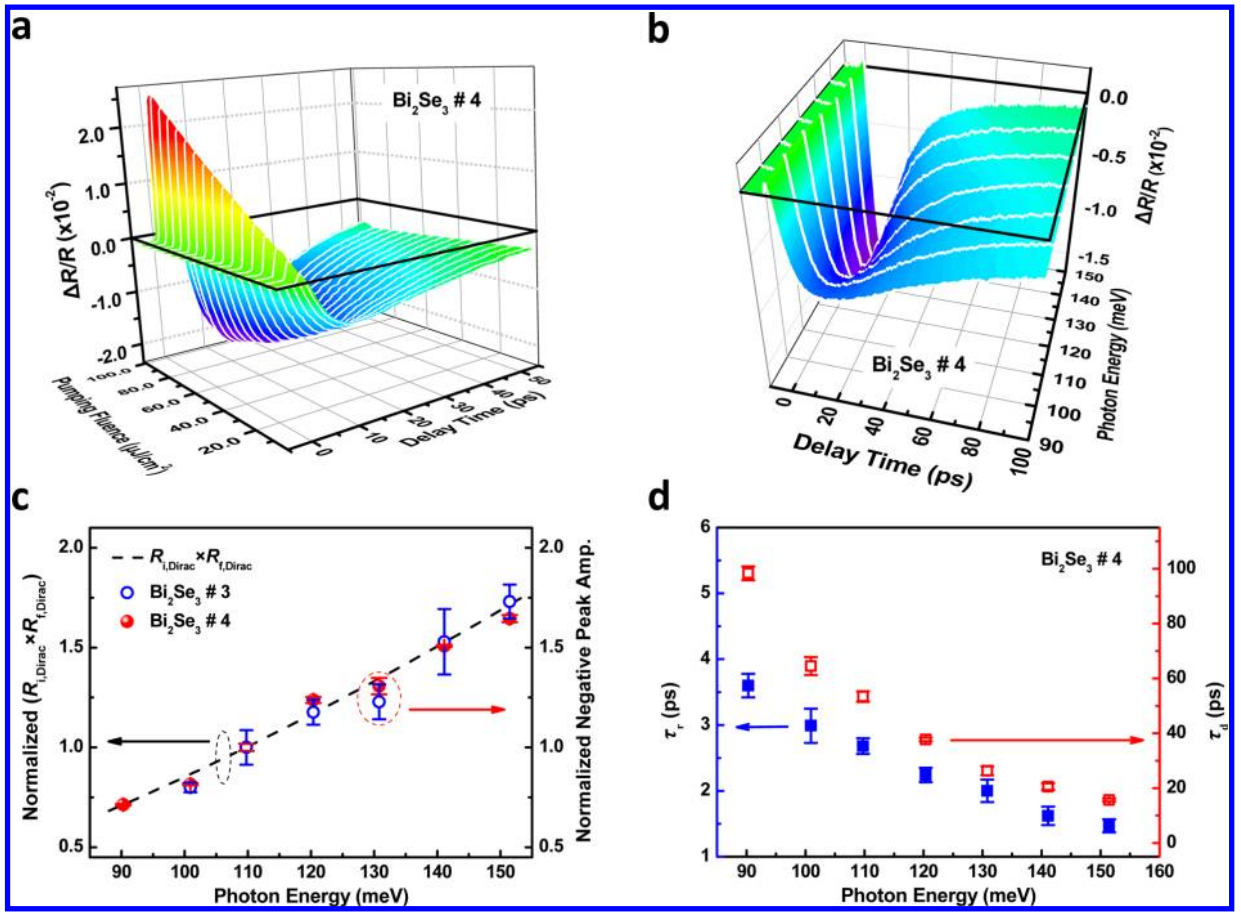

Figure 3. Pumping fluence and photon energy dependence of $\Delta R/R$ and its amplitude and rising (decay) time in the surface state. (a) With probing photon energy of 141 meV, the $\Delta R/R$ of Bi_2Se_3 #4 at various pumping fluences from 3.3−105 $\mu J/cm^2$. (b) With a pumping fluence of 3.3 $\mu J/cm^2$, the $\Delta R/R$ of Bi_2Se_3 #4 at various photon energies from 90−152 meV. (c) The photon energy-dependent negative peak amplitude of $\Delta R/R$ in panel b. The photon energy dependence of the normalized absorption probability (dashed line, that is, $R_{i,Dirac} \times R_{f,Dirac}$ in Figure 2a) of the mid-IR probe beam in the Dirac cone surface state. (d) The photon energy-dependent rising time (τ_r) and decay time (τ_d) of $\Delta R/R$ in (b).

Phonons have been considered as the main medium in the relaxation of Dirac fermions.[14,28−31] Here, we follow this approach. The photon energy dependence of the rising time implies the coupling strength (λ) between Dirac fermions and phonons varies at different positions of the Dirac cone. According to the second moment of the Eliashberg function,[32] the λ is inversely proportional to the relaxation time (τ_e) of excited electrons

$$\lambda\langle\omega^2\rangle \propto \frac{1}{\tau_e} \quad (1)$$

where ω is the phonon energy that couples with the electrons. For the estimate of $\langle\omega^2\rangle$, some vibrational modes are more efficiently coupled to Dirac fermions than others are. In the case of Bi_2Se_3, the symmetric A_{1g}^1 mode of ∼8.9 meV is coherently excited by photoexcitation and efficiently coupled.[21,33] Taking $\tau_e = \tau_r$ in Figure 3d and T_e = 370 K (obtained from ref 14 at the low pumping fluence as mentioned above) to estimate the coefficient of $(\pi k_B T_e/3\hbar)$ in eq 1, the photon energy dependence of the Dirac fermion-phonon coupling strength is λ = 0.08 to 0.19, as shown in Figure 4a. Recently, the ARPES measurements have reported inconsistent electron−phonon coupling strength in Bi_2Se_3 varying from a rather small λ∼0.08[30] to a larger λ∼0.25.[31] The Dirac fermion−phonon coupling strength measured by the present OPMP becomes significantly smaller near the Dirac point (the point of $K_{//}$ = 0 in Figure 4a), which has a qualitatively similar tendency to the estimate of equation 8 (dashed line in Figure 4a) in ref 29. The present results suggest that the variation of λ from ARPES may be due to the different explored regimes (i.e., the different chemical potentials) in the Dirac cone. Besides, the time-resolved ARPES experiments also showed similar results. Wang et al.[14] reported that the surface cooling rate decrease with the Fermi level (i.e., closing to the Dirac point). Because the cooling time is inversely proportional to the surface cooling rate, these time-resolved ARPES results are consistent with those in Figure 3d. If the Dirac fermions are closer to the Dirac point, they will have weaker coupling with the phonons to suppress the scattering with phonons. This also implies the effective mass of Dirac fermions in the surface state gradually decreases as the Dirac fermions approach the Dirac point, in agreement with the results in graphene.[34] Consequently, this study further provides a possibility to control the characteristics of Dirac fermions for various applications in TIs such as terahertz optoelectronics, spintronics, quantum computation, and magnetic memories.

Finally, a closer look at the 3D plot of $-\Delta R/R$ as a function of photon energy at various delays in Figure 4b reveals the absorption peak (marked by arrows in Figure 4b) suffers a red shift with the time delay. This implies the unoccupied density of states in the Dirac cone shift as a function of time, that is, the energy of carrier loss as a function of time. According to the

dx.doi.org/10.1021/nl4021842 | Nano Lett. 2013, 13, 5797−5802

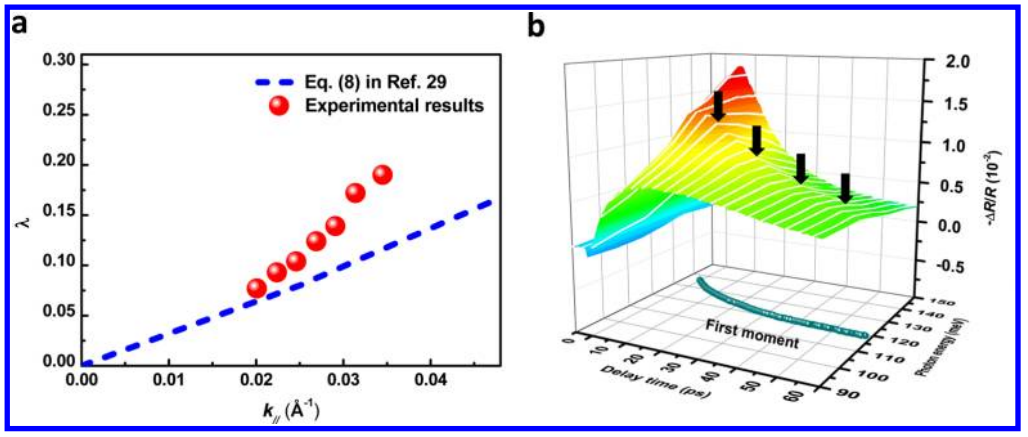

Figure 4. Dirac fermion−phonon coupling strength as a function of momentum and photon energy dependence of the first moment. (a) Momentum-dependent electron−phonon coupling strength (λ) in Dirac cone surface state and compared with the theoretical results (dashed line) from ref 29. (b) Three dimensional plot of the $-\Delta R/R$ in Figure 3b as a function of photon energy at various time delays and the time-dependent first moment (solid dots). The arrows mark the position of absorption peaks at different delay time.

first moment, $(\int(\Delta R/R)E_{photon}\, dE_{photon})/(\int(\Delta R/R)dE_{photon})$, we estimate the energy loss rate of carriers in the Dirac cone. As shown in Figure 4b, the solid dots represent the first moment at different time, which is associated with the red shift of the absorption peak in Figure 4b. An exponential fit to the time-dependent first moment in Figure 4b gives a relaxation time of 14.8 ps within the range of 15 meV. Therefore, the energy loss rate of Dirac fermions in the Dirac cone is ∼1 meV/ps, which is larger than that of ∼0.64 meV/ps in GaAs estimated from ref 25 but smaller than that of ∼17.7 meV/ps in graphene with Dirac cone.[35] This parameter measured by OPMP would be extremely important for designing optoelectronics, especially in the terahertz range.

■ ASSOCIATED CONTENT

Supporting Information

Sample preparation and experimental details on optical pump mid-infrared probe spectroscopy. Angle-resolved photoemission spectroscopy and determining the carrier concentration of surface and bulk states. The physical origin of positive and negative signals in $\Delta R/R$. This material is available free of charge via the Internet at http://pubs.acs.org.

■ AUTHOR INFORMATION

Corresponding Authors

*E-mail: (C.W.L.) cwluo@mail.nctu.edu.tw.
*E-mail: (J.-Y.L.) ago@cc.nctu.edu.tw

Notes

The authors declare no competing financial interest.

The authors declare no competing financial interest.

■ ACKNOWLEDGMENTS

This work was supported by the National Science Council of the Republic of China, Taiwan (Contract No. NSC101-2112-M-009-016-MY2, NSC 101-2112-M-009-017-MY2, NSC 102-2112-M-009-006-MY3, NSC101-2009-M-002-007), the Grant MOE ATU Program at NCTU and RFBR Project 12-02-33174 d. The work at BNL was supported by U.S. Department of Energy, under Contract No. DEAC02- 98CH10886.

■ REFERENCES

(1) Hsieh, D.; Qian, D.; Wray, L.; Xia, Y.; Hor, Y. S.; Cava, R. J.; Hasan, M. Z. A topological Dirac insulator in a quantum spin Hall phase. *Nature* **2008**, *452*, 970−974.
(2) Hasan, M. Z.; Kane, C. L. Colloquium: Topological insulators. *Rev. Mod. Phys.* **2010**, *82*, 3045−3067.
(3) Qi, X.-L.; Zhang, S.-C. Topological insulators and superconductors. *Rev. Mod. Phys.* **2011**, *83*, 1057−1110.
(4) Xia, Y.; Qian, D.; Hsieh, D.; Wray, L.; Pal, A.; Lin, H.; Bansil, A.; Grauer, D.; Hor, Y. S.; Cava, R. J.; Hasan, M. Z. Observation of a large-gap topological-insulator class with a single Dirac cone on the surface. *Nat. Phys.* **2009**, *5*, 398−402.
(5) Hsieh, D.; et al. A tunable topological insulator in the spin helical Dirac transport regime. *Nature* **2009**, *460*, 1101−1106.
(6) Chen, Y. L.; et al. Experimental realization of a three-dimensional topological insulator, Bi_2Te_3. *Science* **2009**, *325*, 178−181.
(7) Zhang, T.; et al. Experimental demonstration of topological surface states protected by time-reversal symmetry. *Phys. Rev. Lett.* **2009**, *103*, 266803.
(8) Roushan, P.; Seo, J.; Parker, C. V.; Hor, Y. S.; Hsieh, D.; Qian, D.; Richardella, A.; Hasan, M. Z.; Cava, R. J.; Yazdani, A. Topological surface states protected from backscattering by chiral spin texture. *Nature* **2009**, *460*, 1106−1110.
(9) Alpichshev, Z.; Analytis, J. G.; Chu, J.-H.; Fisher, I. R.; Chen, Y. L.; Shen, Z. X.; Fang, A.; Kapitulnik, A. STM imaging of electronic waves on the surface of Bi_2Te_3: topologically protected surface states and hexagonal warping effects. *Phys. Rev. Lett.* **2010**, *104*, 016401.
(10) Kim, S.; et al. Surface scattering via bulk continuum states in the 3D topological insulator Bi_2Se_3. *Phys. Rev. Lett.* **2011**, *107*, 056803.
(11) Hsieh, D.; McIver, J. W.; Torchinsky, D. H.; Gardner, D. R.; Lee, Y. S.; Gedik, N. Nonlinear optical probe of tunable surface electrons on a topological insulator. *Phys. Rev. Lett.* **2010**, *106*, 057401.
(12) Sobota, J. A.; Yang, S.; Analytis, J. G.; Chen, Y. L.; Fisher, I. R.; Kirchmann, P. S.; Shen, Z.-X. Ultrafast optical excitation of a persistent surface-state population in the topological insulator Bi_2Se_3. *Phys. Rev. Lett.* **2012**, *108*, 117403.
(13) Hajlaoui, M.; et al. Ultrafast Surface Carrier Dynamics in the Topological Insulator Bi_2Te_3. *Nano Lett.* **2012**, *12*, 3532−3536.
(14) Wang, Y. H.; Hsieh, D.; Sie, E.; Steinberg, H.; Gardner, D.; Lee, Y.; Jarillo-Herrero, P.; Gedik, N. Measurement of intrinsic Dirac fermion cooling on the surface of the topological insulator Bi_2Se_3 using time-resolved and angle-resolved photoemission spectroscopy. *Phys. Rev. Lett.* **2012**, *109*, 127401.
(15) Aguilar, R. V.; et al. Terahertz response and colossal Kerr rotation from the surface states of the topological insulator Bi_2Se_3. *Phys. Rev. Lett.* **2012**, *108*, 087403.

(16) LaForge, A. D.; Frenzel, A.; Pursley, B. C.; Lin, T.; Liu, X.; Shi, J.; Basov, D. N. Optical characterization of Bi_2Se_3 in a magnetic field: Infrared evidence for magnetoelectric coupling in a topological insulator material. *Phys. Rev. B* **2010**, *81*, 125120.
(17) Kamaraju, N.; Kumar, S.; Sood, A. K. Temperature-dependent chirped coherent phonon dynamics in Bi_2Te_3 using high-intensity femtosecond laser pulses. *Europhys. Lett.* **2010**, *92*, 47007.
(18) Qi, J.; et al. Ultrafast carrier and phonon dynamics in Bi_2Se_3 crystals. *Appl. Phys. Lett.* **2010**, *97*, 182102.
(19) Kumar, N.; Ruzicka, B. A.; Butch, N. P.; Syers, P.; Kirshenbaum, K.; Paglione, J.; Zhao, H. Spatially resolved femtosecond pump-probe study of topological insulator Bi_2Se_3. *Phys. Rev. B* **2011**, *83*, 235306.
(20) Hsieh, D.; Mahmood, F.; McIver, J. W.; Gardner, D. R.; Lee, Y. S.; Gedik, N. Selective probing of photoinduced charge and spin dynamics in the bulk and surface of a topological insulator. *Phys. Rev. Lett.* **2011**, *107*, 077401.
(21) Chen, H.-J.; et al. Phonon dynamics in $Cu_xBi_2Se_3$ (x = 0, 0.1, 0.125) and Bi_2Se_2 crystals studied using femtosecond spectroscopy. *Appl. Phys. Lett.* **2012**, *101*, 121912.
(22) Kim, K. W.; Pashkin, A.; Schäfer, H.; Beyer, M.; Porer, M.; Wolf, T.; Bernhard, C.; Demsar, J.; Huber, R.; Leitenstorfer, A. Ultrafast transient generation of spin-density-wave order in the normal state of $BaFe_2As_2$ driven by coherent lattice vibration. *Nat. Mater.* **2012**, *11*, 497−501.
(23) Pashkin, A.; et al. Femtosecond response of quasiparticles and phonons in superconducting $YBa_2Cu_3O_{7-\delta}$ studied by wideband terahertz spectroscopy. *Phys. Rev. Lett.* **2010**, *105*, 067001.
(24) Luo, C. W. THz Generation and Detection on Dirac Fermions in Topological Insulators. *Adv. Opt. Mater.* **2013**.
(25) van Dantzig, N. A.; Planken, P. C. M. Time-resolved far-infrared reflectance of n-type GaAs. *Phys. Rev. B* **1999**, *59*, 1586.
(26) If one absorbed photon generates one photoinduced carrier, the maximum phtotinduced carrier density can be estimated by $\Delta n = (1 - R) \times F/(E \times \delta)$, where R = 0.55 is the reflectance, F = 3.3 μJ/cm^2 is pumping fluence, $E = 2.48 \times 10^{-19}$ J (= 1.55 eV) is the pumping photon energy, δ = 23.5 nm is the penetration depth. For the pumping fluence of 3.3 μJ/cm^2, the photoinduced carrier density Δn is around 2.54×10^{18} cm^{-3}. Figure S12 in Supporting Information further shows that the pump−probe experiments were performed at the weak perturbation limit and the linear response. Additionally, the interband transitions between BVB and BCB dominate the excitation process as discussed in the section S9 of Supporting Information. This indicates that most carriers in BCB and surface states still keep "cold" during pumping.
(27) The electrons and holes in Dirac cone also possibly recombine cross the Dirac point. However, the asymmetric decay of carrier population in Dirac cone observed by time-resolved ARPES experiment[13] has demonstrated that the phonon-assisted cooling of hot carriers is the main relaxation process, which is the focus point in this study.
(28) Zhu, X.; Santos, L.; Sankar, R.; Chikara, S.; Howard, C.; Chou, F. C.; Chamon, C.; El-Batanouny, M. Interaction of phonons and Dirac fermions on the surface of Bi_2Se_3: a strong Kohn anomaly. *Phys. Rev. Lett.* **2011**, *107*, 186102.
(29) Zhu, X.; Santos, L.; Howard, C.; Sankar, R.; Chou, F. C.; Chamon, C.; El-Batanouny, M. Electron-phonon coupling on the surface of the topological insulator Bi_2Se_3 determined from surface-phonon dispersion measurements. *Phys. Rev. Lett.* **2012**, *108*, 185501.
(30) Pan, Z.-H.; Fedorov, A. V.; Gardner, D.; Lee, Y. S.; Chu, S.; Valla, T. Measurement of an exceptionally weak electron-phonon coupling on the surface of the topological insulator Bi_2Se_3 using angle-resolved photoemission spectroscopy. *Phys. Rev. Lett.* **2012**, *108*, 187001.
(31) Hatch, R. C.; Bianchi, M.; Guan, D.; Bao, S.; Mi, J.; Iversen, B. B.; Nilsson, L.; Hornekær, L.; Hofmann, P. Stability of the Bi_2Se_3(111) topological state: Electron-phonon and electron-defect scattering. *Phys. Rev. B* **2011**, *83*, 241303 (R).
(32) Allen, P. B. Theory of thermal relaxation of electrons in metals. *Phys. Rev. Lett.* **1987**, *59*, 1460.
(33) Chis, V.; Sklyadneva, I. Y.; Kokh, K. A.; Volodin, V. A.; Tereshchenko, O. E.; Chulkov, E. V. Vibrations in binary and ternary topological insulators: first-principles calculations and Raman spectroscopy measurements. *Phys. Rev. B* **2012**, *86*, 174304.
(34) Novoselov, K. S.; Geim, A. K.; Morozov, S. V.; Jiang, D.; Katsnelson, M. I.; Grigorieva, I. V.; Dubonos, S. V.; Firsov, A. A. Two-dimensional gas of massless Dirac fermions in graphene. *Nature* **2005**, *438*, 197−200.
(35) Luo, C. W.; et al. Dirac fermion-phonon coupling and energy loss rate near Fermi surface in monolayer and multilayer graphene. Unpublished work, 2013.